Fluid Mechanics Report

Rotationally Invariant Grid-less Upwind Method for Euler Equations

Praveen C and S M Deshpande

CFD Center, Department of Aerospace Engg.,

Indian Institute of Science, Bangalore

Abstract

A new Kinetic Rotationally Invariant Method for Euler equations (KRIME) based on least squares is described on arbitrary grids. Unlike LSKUM, the new method does not split the stencil for achieving upwinding but uses the full stencil. Upwinding is achieved in a novel way which is possible due to the kinetic framework. The method can be applied to any system of conservation laws which have a kinetic representation.

1 Introduction

The LSKUM of Ghosh [5] is an upwind method for Euler equations on arbitrary grids. This method has been shown to work on arbitrary distribution of points and for a variety of flow situations [9]. Upwinding is enforced at the level of kinetic theory by splitting the velocity space and the stencil. The splitting of the stencil may lead to problems due to insufficient number or absence of points in a half stencil. Though this problem can be solved by stencil augmentation it is still advantageous to have a grid-free method which does not require such correction of stencil. Hence it is pertinent to ask the following question.
Question: Is it possible to develop a numerical method for the Euler equations which,

1. is grid-less,
2. is upwind,
3. uses full stencil,
4. is multi-dimensional.

There are two methods known to the authors which satisfy some if not all of these conditions. These are the LSFD-U of Balakrishnan[1, 2, 7] and the gridless method of Morinishi [6]. Both these approaches do not make use of the kinetic formalism and can be used either in the framework of flux-vector splitting or flux-difference splitting. Here, we are interested in exploiting the connection between the Boltzmann equation and the Euler equations in developing a new method which satisfies all the above four conditions. We also establish

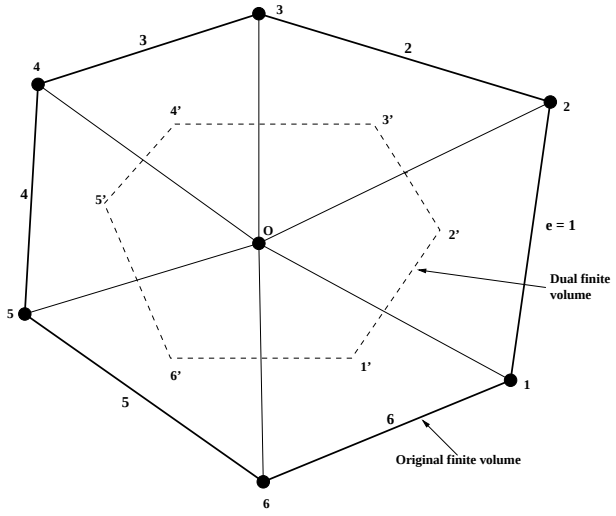

Figure 1: Finite volume definition

the rotational invariance of the method which is a requirement of any genuinely multi-dimensional upwind method. The scheme is first described in one-dimension together with analysis of the consistency of the scheme. The extension to two-dimensions is then given which is non-trivial. Numerical results are presented only for the two-dimensional case.

2 Finite volume schemes

Consider a finite volume approximation of a scalar conservation law

$$\frac{\partial u}{\partial t} + \nabla \cdot \vec{F} = 0$$

Assume that the data is stored at the vertices of a grid. For a node o, we can construct a finite volume Ω using the nodes $1, 2, 3, 4, 5, 6$ as shown in figure (1). The integral form of the conservation law is

$$\frac{\partial}{\partial t} \int_\Omega u \mathrm{d}V + \int_{\partial\Omega} \vec{F} \cdot \hat{n} \mathrm{d}S = 0$$

which for the finite volume can be written as

$$\frac{\partial}{\partial t} \int_\Omega u \mathrm{d}V + \sum_{e=1}^{6} \int_e \vec{F} \cdot \hat{n} \mathrm{d}S = 0$$

where e denotes an edge of the finite volume. A simple way to evaluate the integrals in the above equation is to use trapezoidal rule

$$\int_e \vec{F} \cdot \hat{n} \mathrm{d}S \approx \frac{1}{2}[\vec{F}_e + \vec{F}_{e+1}] \cdot \hat{n}_e S_e$$

with the convention that

$$(\vec{F} \cdot \hat{n})_7 = (\vec{F} \cdot \hat{n})_1$$

Such a scheme would correspond to central differencing which is known to be unstable for hyperbolic problems since they do not have the upwind property. To derive a stable scheme, the concept of *dual finite volume* is used. One example of a dual cell is shown in figure (1) which is formed by the perpendicular bisectors of the lines joining the vertices. The integral form of the conservation law is now applied to the dual cell. The fluxes across the edges $1'2'$, $2'3'$, ..., have to be evaluated. For the dual cell the data is discontinuous across each edge and a flux-vector or flux-difference splitting method, which are based on some upwind principle, is used to evaluate the flux. We see that the use of dual cells stabilizes the scheme by the introduction of discontinuities. In the present work which is based on least squares, a similar situation arises. In order to introduce some upwinding the data on the given stencil is transferred onto a *dual stencil*. The exact details are given in section (4).

3 One Dimensional Case

Consider a one-dimensional arbitrary distribution of points and let o be a typical node, with its connectivity[1] $\mathcal{C}_o = \{i : 1 \leq i \leq N_o\}$, which we call the *primary stencil*. For later use, we introduce the following notation: $\mathcal{L}_o = \{i \in \mathcal{C}_o : x_i < x_o\}$ and $\mathcal{R}_o = \mathcal{C}_o - \mathcal{L}_o$. Let f be a scalar function specified at these nodes and let I denote the mid-point of the line segment oi. We will call the set of all such points I obtained from a primary stencil to form the *dual stencil*. Using Taylor's formula, we can write the Taylor's series for the exact value of f at I, denoted by f_I^e, as,

$$f_I^e = f_o + \Delta x_I \left(\frac{\mathrm{d}f}{\mathrm{d}x}\right)_o + \frac{{\Delta x_I}^2}{2!}\left(\frac{\mathrm{d}^2 f}{\mathrm{d}x^2}\right)_o + ...$$

Let us retain terms upto order l in the above formula, and define an error,

$$E_I = f_I^e - \left[f_o + \Delta x_I \left(\frac{\mathrm{d}f}{\mathrm{d}x}\right)_o + \frac{{\Delta x_I}^2}{2!}\left(\frac{\mathrm{d}^2 f}{\mathrm{d}x^2}\right)_o + ... + \frac{{\Delta x_I}^l}{l!}\left(\frac{\mathrm{d}^l f}{\mathrm{d}x^l}\right)_o\right]$$

If we know f_I^e, then we can use the least squares principle and obtain an l-th order accurate estimate of f_x at node o. Since we do not know f_I^e, let us assume that we can obtain a k-exact approximation to it, denoted by f_I, i.e., $f_I^e = f_I + O({\Delta x_I}^{k+1})$. If we want to use f_I in place of f_I^e, then $(f_I^e - f_I)$ must be of the order of the neglected terms in the Taylor expansion, i.e., $k \geq l$. This gives the following result.

Theorem 1 *The l'th order least squares procedure on the dual stencil is consistent if and only if $k \geq l$, and the resulting least squares formula for the gradient is l-exact. As a consequence, if $l = 1$, then the least squares formula is consistent if $k \geq 1$.*

[1] The terms connectivity and stencil are in the same sense.

Hence if we want to use first order least squares formula, then the interpolation for determining f_I must be atleast second order accurate (i.e., linear interpolation).

Remark: The reason for introducing the point I instead of working with i is to achieve upwinding without stencil splitting. The idea is to define a *dual stencil* of points I and then use the least squares formula for the points in the dual stencil. This will become clear in the next section.

Remark: Note that there may be a case where a node I of the dual stencil coincides with a node j of the primary stencil. It would then seem inconsistent to use some other value at the node for evaluation of the derivative. But since by the previous theorem we always need to perform interpolation to obtain the value at I, we will atleast have $f_I - f_j = O(h^2)$ and the error in using f_I instead of f_j will be mathematically acceptable since we are anyway neglecting terms of $O(h^2)$ in our least squares procedure.

4 Numerical Scheme in 1-D

The Euler equation in conservation form is given by,

$$\frac{\partial U}{\partial t} + \frac{\partial F}{\partial x} = 0 \tag{1}$$

where U is the vector of conserved variables and F is the flux vector,

$$U = \begin{bmatrix} \rho \\ \rho u \\ E \end{bmatrix}, \quad F = \begin{bmatrix} \rho u \\ p + \rho u^2 \\ (E+p)u \end{bmatrix}$$

The system of equations (1) can be obtained by taking moments of the Boltzmann equation without the collision term

$$\frac{\partial f}{\partial t} + v\frac{\partial f}{\partial x} = 0 \tag{2}$$

The moments are defined by[2],

$$U = \int \psi f \mathrm{d}v\mathrm{d}I, \quad F = \int v\psi f \mathrm{d}v\mathrm{d}I \tag{3}$$

with ψ being the collisional invariants of the Boltzmann equation and f the Maxwellian distribution. In one-dimension, these are given by,

$$\psi = \begin{bmatrix} 1 \\ v \\ I + \dfrac{v^2}{2} \end{bmatrix}$$

[2]Unless stated otherwise, all integrals are over $\mathbb{R}^d \times \mathbb{R}^+$, where d is the number of spatial dimensions, and $\mathbb{R}^+ = \{x \in \mathbb{R} : x \geq 0\}$.

$$f = \frac{\rho}{I_o}\sqrt{\frac{\beta}{\pi}}\exp\left\{-\beta(v-u)^2 - \frac{I}{I_o}\right\}$$

Equations (2)-(3) give a kinetic representation of the system of conservation laws (1). We will develop a method for (1) starting from the kinetic representation.

In order to estimate the spatial derivative in equation (2), we make use of the technique described in section (3) keeping in mind the result of theorem (1). Assume that f_I is a 1-exact approximation to f_I^e. Then we define the error E_I as,

$$E_I = f_I - f_o - \Delta x_I f_{xo} = \Delta f_I - \Delta x_I f_{xo}$$

where $\Delta(\cdot)_I = (\cdot)_I - (\cdot)_o$. Minimizing,

$$\sum_I E_I^2$$

wrt f_{xo}, we obtain the usual least squares formula,

$$f_{xo}^{[1]} = \frac{\sum \Delta x_I \Delta f_I}{\sum \Delta x_I^2} \tag{4}$$

on the *dual* stencil $\mathcal{C}_o' = \{I : i \in \mathcal{C}_o\}$. The superscript "[1]" denotes that it is a first order formula on the dual stencil.

If f is the velocity distribution function, then the second order upwind estimate for f_I may be obtained in two ways[3].

Case 1:

$$f_I = \begin{cases} f_L + |\Delta x_I| f_{xL}^{(1)}, \text{ if } v \geq 0 \\ \\ f_R - |\Delta x_I| f_{xR}^{(1)}, \text{ if } v \leq 0 \end{cases} \tag{5}$$

Case 2:

$$f_I = \begin{cases} f(\bar{q}_L), \text{ if } v \geq 0 \\ \\ f(\bar{q}_R), \text{ if } v \leq 0 \end{cases} \tag{6}$$

where

$$\bar{q}_L = q_L + |\Delta x_I| q_{xL}^{(1)}$$
$$\bar{q}_R = q_R - |\Delta x_I| q_{xR}^{(1)}$$

The subscripts L and R denote the states to the left and right of I respectively, as shown in figure (2), and the superscript "(1)" denotes that the gradients are obtained using the first order least squares formula with the full *primary* stencil. Substituting equation (4) into the Boltzmann equation and taking moments, we obtain a discrete approximation to the Euler equation,

$$\frac{\mathrm{d}U_o}{\mathrm{d}t} + \frac{\sum \Delta x_I \Delta F_I}{\sum \Delta x_I^2} = 0 \tag{7}$$

[3] See Appendix (A)

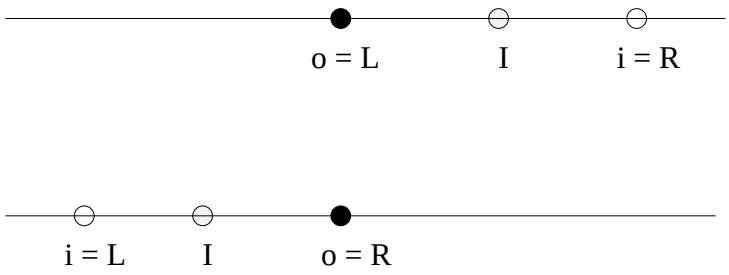

Figure 2: Stencil in 1-D and definition of left/right states.

where the flux F_I is defined as[4],

$$F_I = \int v\psi f_I \mathrm{d}\vec{v}\mathrm{d}I \tag{8}$$

Remark: Upwinding is introduced in the above method by mapping the data on the primary stencil onto a dual stencil *in an upwind manner.* Updating is done by using the data on the dual stencil. If we use the primary stencil, then the only way to achieve upwinding is by stencil splitting as in LSKUM. The use of the dual stencil can be compared with dual finite volumes in a cell-vertex finite volume method as discussed in section (2).

Remark: Strictly speaking the present method is not upwind but may be called *upwind biased.* The main reason for this is the absence of a first order method which makes use of only upwind data; even the first order scheme requires interpolation through a least squares formula which brings in downwind effect. We will however still continue to call it an upwind method and the numerical results to be presented make allowance for our misuse of terminology.

Remark: The update formula (7) is identical to that of LSFD-U. The fluxes F_I are evaluated here based on a splitting of the velocity-space at the level of kinetic theory, while in LSFD-U, the fluxes can be evaluated using any flux-vector or flux-difference splitting method.

5 Further Analysis

We have seen that if we use first order least squares procedure together with point values for evaluating f at the points I in the dual stencil, then we get an inconsistent formula. To demonstrate this more explicitly, let us use the following approximation to f_I in equation (4),

$$f_I = \begin{cases} f_L, \text{ if } v \geq 0 \\ \\ f_R, \text{ if } v \leq 0 \end{cases} \tag{9}$$

[4]The I in f_I is not related to the I in $\mathrm{d}I$.

Substituting equation (4) into the Boltzmann equation, we get,

$$\int \psi \frac{\partial f}{\partial t} \mathrm{d}\vec{v}\mathrm{d}I + \int v\psi \frac{\sum \Delta x_I \Delta f_I}{\sum \Delta x_I^2} \mathrm{d}\vec{v}\mathrm{d}I = \frac{\mathrm{d}U_o}{\mathrm{d}t} + \frac{\sum \Delta x_I \Delta F_I}{\sum \Delta x_I^2} = 0$$

Making use of the fact that,

$$v f_I = \frac{v + |v|}{2} f_L + \frac{v - |v|}{2} f_R$$

we get the following expression for F_I,

$$F_I = \begin{cases} F_o^+ + F_i^-, \text{ if } i \in \mathcal{R}_o \\ \\ F_i^+ + F_o^-, \text{ if } i \in \mathcal{L}_o \end{cases}$$

so that we obtain,

$$\frac{\sum \Delta x_I \Delta F_I}{\sum \Delta x_I^2} = \frac{(\sum \Delta x_I \Delta F_i^+)_{i \in \mathcal{R}_o} + (\sum \Delta x_I \Delta F_i^-)_{i \in \mathcal{L}_o}}{(\sum \Delta x_I^2)_{i \in \mathcal{R}_o \cup \mathcal{L}_o}}$$

Let,

$$a_o = \sum_{i \in \mathcal{L}_o} \Delta x_I^2, \quad b_o = \sum_{i \in \mathcal{R}_o} \Delta x_I^2$$

Using Taylor's formula, we can write,

$$\Delta F_i^{\pm} = 2\Delta x_I F_{xo}^{\pm} + O(\Delta x_I^2)$$

Substituting this and the definition of a, b, we get,

$$\frac{\sum \Delta x_I \Delta F_I}{\sum \Delta x_I^2} = \frac{2b_o F_{xo}^+ + 2a_o F_{xo}^-}{a_o + b_o} + O(h)$$

This can be rearranged as,

$$\frac{\sum \Delta x_I \Delta F_I}{\sum \Delta x_I^2} = F_{xo} + \left(\frac{a_o - b_o}{a_o + b_o} \right) (F_{xo}^- - F_{xo}^+) + O(h) \tag{10}$$

In general, the second term on the right is $O(1)$ which makes the formula inconsistent. It will be consistent only if $a_o = b_o$. Consider for example, the following stencil,

$$\{x_o - 3h, x_o - h, x_o, x_o + h, x_o + 2h\}$$

This gives,

$$\frac{\sum \Delta x_I \Delta F_I}{\sum \Delta x_I^2} = F_{xo} + \frac{1}{3}(F_{xo}^- - F_{xo}^+) + O(h)$$

Clearly, this shows that the formula is inconsistent since the error is of $O(1)$ even in the limit of $h \to 0$. In general, a necessary and sufficient condition for consistency is that for some $\alpha > 0$

$$a_o - b_o = O(h^{2+\alpha}) \tag{11}$$

Since $a_o + b_o = O(h^2)$, we see that the second term on the right of equation (10) is $O(h^\alpha)$ and the order of accuracy of the formula is $\min(1, \alpha)$.

In the previous section, a consistent first order scheme has been constructed but it makes use of the least squares formula on the primary stencil to get a consistent estimate of f_x. These gradients are then used to obtain a consistent least squares formula for the gradient, which operates on the dual stencil and is also first order accurate.

Remark: The discussion in the above section shows that the least squares formula on the dual stencil can be consistent in some cases even when no interpolation is performed for determining the values at the dual nodes. Even though the final result makes sense, the least squares procedure itself is mathematically inconsistent since we would be introducing errors of order higher than those which are neglected in the Taylor's formula. Note that theorem (1) states the necessary and sufficient condition for the *mathematical consistency of the least squares procedure* and only gives the sufficient condition for the consistency of the least squares formula.

6 Numerical Scheme in 2-D

The result of theorem (1) is valid in the two-dimensional case also. Hence we derive a formally first order accurate method by making use of linear interpolation for the fluxes. The 2-D Euler equation in conservation form is,

$$\frac{\partial U}{\partial t} + \frac{\partial F}{\partial x} + \frac{\partial G}{\partial y} = 0 \tag{12}$$

where U is the vector of conserved variables and F, G are the cartesian components of the flux.

$$U = \begin{bmatrix} \rho \\ \rho u_1 \\ \rho u_2 \\ E \end{bmatrix}, \quad F = \begin{bmatrix} \rho u_1 \\ p + \rho u_1^2 \\ \rho u_1 u_2 \\ (E+p) u_1 \end{bmatrix}, \quad G = \begin{bmatrix} \rho u_2 \\ \rho u_1 u_2 \\ p + \rho u_2^2 \\ (E+p) u_2 \end{bmatrix}$$

The system of equations (12) can be obtained by taking moments of the Boltzmann equation without the collision term

$$\frac{\partial f}{\partial t} + v_1 \frac{\partial f}{\partial x} + v_2 \frac{\partial f}{\partial y} = 0 \tag{13}$$

The moments are defined by,

$$U = \int \psi f \mathrm{d}\vec{v}\mathrm{d}I, \quad F = \int v_1 \psi f \mathrm{d}\vec{v}\mathrm{d}I, \quad G = \int v_2 \psi f \mathrm{d}\vec{v}\mathrm{d}I \tag{14}$$

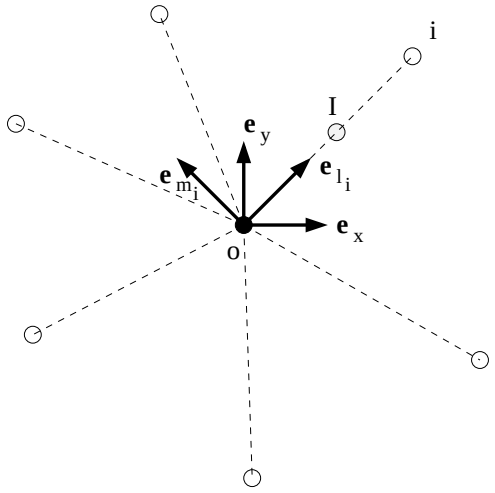

Figure 3: Stencil in 2-D and definition of unit vectors.

with ψ being the collisional invariants of the Boltzmann equation and f the Maxwellian distribution. In two-dimensions, these are given by,

$$\psi = \begin{bmatrix} 1 \\ v_1 \\ v_2 \\ I + \frac{1}{2}|\vec{v}|^2 \end{bmatrix}$$

$$f = \frac{\rho}{I_o}\frac{\beta}{\pi}\exp\left\{-\beta|\vec{v}-\vec{u}|^2 - \frac{I}{I_o}\right\}$$

6.1 Least Squares Principle

Consider a typical node o and it's stencil $\{i : 1 \leq i \leq N_o\}$. Let I denote the midpoint of the line segment $\vec{oi}$. Let the unit vectors along and normal to $\vec{oi}$ be denoted as $\vec{e}_{li}$ and $\vec{e}_{mi}$. Figure (3) gives a definition sketch. If (l_i, m_i) are the direction cosines of $\vec{oi}$, then

$$\begin{aligned} \vec{e}_{li} &= l_i\vec{e}_x + m_i\vec{e}_y \\ \vec{e}_{mi} &= -m_i\vec{e}_x + l_i\vec{e}_y \end{aligned}$$

Assume that f_I is a 1-exact upwind approximation to f_I^e in the sense of section (4). Then, similar to 1-D case, we define the error E_I as,

$$\begin{aligned} E_I &= f_I - f_o - \Delta x_I f_{xo} - \Delta y_I f_{yo} \\ &= \Delta f_I - \Delta x_I f_{xo} - \Delta y_I f_{yo} \end{aligned}$$

Minimizing,

$$\sum_I w_I E_I^2$$

wrt f_{xo}, f_{yo}, we obtain the usual least squares formula,

$$f_{xo}^{[1]} = \frac{\sum w_I \Delta y_I^2 \sum w_I \Delta x_I \Delta f_I - \sum w_I \Delta x_I \Delta y_I \sum w_I \Delta y_I \Delta f_I}{\sum w_I \Delta x_I^2 \sum w_I \Delta y_I^2 - (\sum w_I \Delta x_I \Delta y_I)^2} \tag{15}$$

$$f_{yo}^{[1]} = \frac{\sum w_I \Delta x_I^2 \sum w_I \Delta y_I \Delta f_I - \sum w_I \Delta x_I \Delta y_I \sum w_I \Delta x_I \Delta f_I}{\sum w_I \Delta x_I^2 \sum w_I \Delta y_I^2 - (\sum w_I \Delta x_I \Delta y_I)^2} \tag{16}$$

on the dual stencil. We have also introduced a positive weighting function w_I which is a function of $|\vec{x}_I - \vec{x}_o|$. Similar to equation (5)-(6), we can write the second order estimates for f_I as

Case 1:

$$f_I = \begin{cases} f_o + \Delta x_I f_{xo}^{(1)} + \Delta y_I f_{yo}^{(1)}, \text{ if } v_l \geq 0 \\ \\ f_i - \Delta x_I f_{xi}^{(1)} - \Delta y_I f_{yi}^{(1)}, \text{ if } v_l \leq 0 \end{cases} \tag{17}$$

Case 2:

$$f_I = \begin{cases} f(q_{oi}), \text{ if } v_l \geq 0 \\ \\ f(q_{io}), \text{ if } v_l \leq 0 \end{cases} \tag{18}$$

where

$$q_{oi} = R_i(q_o + \Delta x_I q_{xo}^{(1)} + \Delta y_I q_{yo}^{(1)})$$

$$q_{io} = R_i(q_i - \Delta x_I q_{xi}^{(1)} - \Delta y_I q_{yi}^{(1)})$$

and R_i is the transformation matrix given by,

$$R_i = \begin{bmatrix} 1 & 0 & 0 & 0 \\ 0 & l_i & m_i & 0 \\ 0 & -m_i & l_i & 0 \\ 0 & 0 & 0 & 1 \end{bmatrix}$$

Here we are assuming that the first and last elements of q are scalars and the middle elements form a vector. Examples of this are the conserved variables $U = (\rho,\ \rho\vec{u},\ E)^t$, the primitive variables $V = (\rho,\ \vec{u},\ p)^t$ or the entropy variables given by equation (32). The effect of multiplying by this matrix is to transform the vector components into the rotated frame. Substituting equation (15)-(16) into the Boltzmann equation and taking moments, we obtain a discrete least squares based approximation to the Euler equations.

$$\frac{\mathrm{d}U_o}{\mathrm{d}t} + \left(\frac{\sum w_I \Delta y_I^2 \sum w_I \Delta x_I \Delta F_I - \sum w_I \Delta x_I \Delta y_I \sum w_I \Delta y_I \Delta F_I}{\sum w_I \Delta x_I^2 \sum w_I \Delta y_I^2 - (\sum w_I \Delta x_I \Delta y_I)^2} \right) + \left(\frac{\sum w_I \Delta x_I^2 \sum w_I \Delta y_I \Delta G_I - \sum w_I \Delta x_I \Delta y_I \sum w_I \Delta x_I \Delta G_I}{\sum w_I \Delta x_I^2 \sum w_I \Delta y_I^2 - (\sum w_I \Delta x_I \Delta y_I)^2} \right) = 0 \tag{19}$$

6.2 Evaluation of Fluxes

In the update equation (19), we have to evaluate the following integrals,

$$\Delta F_I := \int v_1 \psi \Delta f_I \mathrm{d}\vec{v}\mathrm{d}I = \int v_1 \psi f_I \mathrm{d}\vec{v}\mathrm{d}I - \int v_1 \psi f_o \mathrm{d}\vec{v}\mathrm{d}I =: F_I - F_{oi} \tag{20}$$

and

$$\Delta G_I := \int v_2 \psi \Delta f_I \mathrm{d}\vec{v}\mathrm{d}I = \int v_2 \psi f_I \mathrm{d}\vec{v}\mathrm{d}I - \int v_2 \psi f_o \mathrm{d}\vec{v}\mathrm{d}I =: G_I - G_{oi} \tag{21}$$

with f_I given by equation (17) or (18). It is first convenient to define the following split flux,

$$\tilde{G}^{\pm} = \int_{v_1 \gtrless 0} v_2 \psi f \mathrm{d}\vec{v}\mathrm{d}I \tag{22}$$

and the expressions are given in appendix (B). Since, we can write,

$$v_1 = l_i v_l - m_i v_m, \quad v_2 = m_i v_l + l_i v_m$$

the moment vector ψ becomes,

$$\psi = \begin{bmatrix} 1 \\ l_i v_l - m_i v_m \\ m_i v_l + l_i v_m \\ I + \frac{1}{2}(v_l^2 + v_m^2) \end{bmatrix} \tag{23}$$

In the rest of the report, we assume case (2) for interpolation. Substituting these in equations (20)-(21), we obtain after performing the integrations, the following expressions for the fluxes,

$$\left.\begin{aligned} F_I &= \mathcal{F}(q_{oi}, q_{io}; l_i, m_i) \\ G_I &= \mathcal{G}(q_{oi}, q_{io}; l_i, m_i) \end{aligned}\right\} \tag{24}$$

where,

$$\mathcal{F}(p,q;l,m) = \begin{bmatrix} lF_1(p,q) - m\tilde{G}_1(p,q) \\ l^2F_2(p,q) + m^2\tilde{G}_3(p,q) - 2lmF_3(p,q) \\ (l^2-m^2)F_3(p,q) + lm(F_2(p,q) - \tilde{G}_3(p,q)) \\ lF_4(p,q) - m\tilde{G}_4(p,q) \end{bmatrix} \tag{25}$$

$$\mathcal{G}(p,q;l,m) = \begin{bmatrix} mF_1(p,q) + l\tilde{G}_1(p,q) \\ (l^2-m^2)F_3(p,q) + lm(F_2(p,q) - \tilde{G}_3(p,q)) \\ m^2F_2(p,q) + l^2\tilde{G}_3(p,q) + 2lmF_3(p,q) \\ mF_4(p,q) + l\tilde{G}_4(p,q) \end{bmatrix} \tag{26}$$

In the above equations, we have used the following notation,

$$F(p,q) = F^+(p) + F^-(q), \quad \tilde{G}(p,q) = \tilde{G}^+(p) + \tilde{G}^-(q)$$

Similarly, we have

$$\left.\begin{aligned} F_{oi} &= \mathcal{F}(R_i q_o, R_i q_o; l_i, m_i) \\ G_{oi} &= \mathcal{G}(R_i q_o, R_i q_o; l_i, m_i) \end{aligned}\right\} \tag{27}$$

Remark: The reason for defining F_{oi}, G_{oi} in the above manner is that if we have a uniform flow, then $\Delta F_I = \Delta G_I = 0$, so that uniform flow is preserved.

Remark: The appearance of the fluxes $\tilde{G}$ is a distinguishing feature of this method. Both the flux along the ray $\vec{oi}$ and normal to it appear in the update formula. This must be compared with a finite volume method where only the flux normal to the interface appears in the update formula

Remark: There is no theoretical restriction upon the location of the point I except that it should be on the line segment $\vec{oi}$. In the present work, we have placed the dual point I at the mid-point of the line segment $\vec{oi}$.

7 Rotational Invariance

The method described here can be applied in any cartesian coordinate frame because of the use of least squares formula. It is then pertinent to ask the question as to whether there is any coordinate frame which is optimum in the sense that some relevant norm of the error is minimized. To answer this question, we need to use the transformation properties of the least squares formula which have been established in [8]. Theorem (3) establishes the rotational invariance of the method which implies that there is no optimum coordinate frame; all coordinate frames are equivalent in this sense. This is is one of the desired properties of a genuinely multi-dimensional scheme. We first summarize a few results about the transformation properties of the least squares formula [8].

Theorem 2 *Let ϕ, $\vec{u}$ and σ be scalar, vector and second order tensor field variables respectively. Then*

1. $\Delta\vec{r} \cdot \nabla\phi$ *is an invariant.*
2. $\Delta\vec{r} \cdot \nabla\vec{u}$ *is a vector.*
3. $\nabla \cdot \vec{u}$ *is an invariant.*
4. $\nabla \cdot \sigma$ *is a vector.*

The least squares estimate of the above quantities also have the same properties.

This theorem essentially says that the least squares estimates of the derivatives of scalar, vector and tensor field variables share the transformation properties of the corresponding exact derivatives.

Theorem 3 *The scheme defined by (19), (24), (27) is rotationally invariant, i.e., if* ρ^{n+1}, u_1^{n+1}, u_2^{n+1}, E^{n+1}, *is the update in one coordinate frame and* $\bar{\rho}^{n+1}$, $\bar{u}_1^{n+1}$, $\bar{u}_2^{n+1}$, $\bar{E}^{n+1}$, *in any other frame, then they are related by,*

$$\bar{\rho}^{n+1} = \rho^{n+1}, \quad \bar{E}^{n+1} = E^{n+1}$$

$$\begin{bmatrix} \bar{u}_1^{n+1} \\ \bar{u}_2^{n+1} \end{bmatrix} = \mathcal{R} \begin{bmatrix} u_1^{n+1} \\ u_2^{n+1} \end{bmatrix}$$

where $\mathcal{R}$ *is the transformation matrix between the two frames.*

Proof: By the rotational properties of the least squares formula [8] and summarized in theorem (2), we see that q_{oi}, q_{io} and $R_i q_o$ are invariant. It is then enough to show that the mass and energy fluxes transform like a vector, and the momentum flux transforms like a tensor. Let ϕ be the angle between $\vec{e}_l$ and $\vec{e}_x$. Then $l = \cos\phi$ and $m = \sin\phi$, and define the rotation matrix,

$$\mathcal{R}(\phi) = \begin{bmatrix} \cos\phi & \sin\phi \\ -\sin\phi & \cos\phi \end{bmatrix} \tag{28}$$

With p, q denoting q_{oi} or q_{io}, we can write,

$$\begin{bmatrix} \mathcal{F}_1 \\ \mathcal{G}_1 \end{bmatrix} = \mathcal{R}(\phi)^{-1} \begin{bmatrix} F_1(p,q) \\ \tilde{G}_1(p,q) \end{bmatrix} \tag{29}$$

If the coordinate frame is rotated by an angle θ, then the corresponding fluxes are given by,

$$\begin{aligned} \begin{bmatrix} \bar{\mathcal{F}}_1 \\ \bar{\mathcal{G}}_1 \end{bmatrix} &= \mathcal{R}(\phi-\theta)^{-1} \begin{bmatrix} F_1(p,q) \\ \tilde{G}_1(p,q) \end{bmatrix} \\ &= \mathcal{R}(-\phi+\theta) \begin{bmatrix} F_1(p,q) \\ \tilde{G}_1(p,q) \end{bmatrix} \\ &= \mathcal{R}(-\phi+\theta)\mathcal{R}(\phi) \begin{bmatrix} \mathcal{F}_1 \\ \mathcal{G}_1 \end{bmatrix} \\ &= \mathcal{R}(\theta) \begin{bmatrix} \mathcal{F}_1 \\ \mathcal{G}_1 \end{bmatrix} \end{aligned}$$

We see that $(\mathcal{F}_1, \mathcal{G}_1)$ transforms like a vector under coordinate rotation. This implies that the update of density is independent of the coordinate system. The same proof holds for the energy also.

The proof for the momentum is also similar. The momentum flux is given by,

$$\begin{bmatrix} \mathcal{F}_2 & \mathcal{G}_2 \\ \mathcal{F}_3 & \mathcal{G}_3 \end{bmatrix} = \mathcal{R}(\phi)^{-1} \begin{bmatrix} F_2(p,q) & \tilde{G}_2(p,q) \\ F_3(p,q) & \tilde{G}_3(p,q) \end{bmatrix} \mathcal{R}(\phi) \tag{30}$$

and upon coordinate rotation, we obtain,

$$\begin{bmatrix} \bar{\mathcal{F}}_2 & \bar{\mathcal{G}}_2 \\ \bar{\mathcal{F}}_3 & \bar{\mathcal{G}}_3 \end{bmatrix} = \mathcal{R}(\theta) \begin{bmatrix} \mathcal{F}_2 & \mathcal{G}_2 \\ \mathcal{F}_3 & \mathcal{G}_3 \end{bmatrix} \mathcal{R}(\theta)^t \tag{31}$$

so that the momentum flux transforms like a second order tensor.

Remark: If we use a limiter, then q_{oi}, q_{io} may not be invariant since the limiter could depend on the coordinate system. However, this effect has been found to be small and we give a numerical example in support of this remark.

8 Choice of Variable for Interpolation

There are various choices for the variables q_{oi}, q_{io} which are obtained through linear interpolation. In the present framework of splitting the velocity-space the natural choice is the conserved variables. However the use of conserved variables does not ensure the positivity of pressure after a limiting procedure. Hence, it is better to use either the primitive variables $(\rho, \vec{u}, p)$ or the entropy variables which are also known as q-variables [4] and are given by,

$$q = \begin{bmatrix} \ln \rho + \dfrac{\ln \beta}{\gamma - 1} - \beta |\vec{u}|^2 \\ 2\beta \vec{u} \\ -2\beta \end{bmatrix} \tag{32}$$

The use of entropy variables seems to be attractive since it is directly related to the entropy condition.

9 Selection of Stencil

The least squares formula operates on an arbitrary distribution of points for evaluating the derivatives. Hence the selection of a suitable stencil becomes important. First of all, there must be atleast three points in the stencil since the least squares procedure will not be over-determined otherwise. Secondly, all the points in the stencil should not lie along a straight line which would make it impossible to obtain the derivatives normal to that line. Thirdly, the spatial dimensions of the stencil should be small in order to reduce the numerical error. A useful criterion to check the above condition is the *condition number* σ of the least squares matrix [8]. A condition number $\sigma \approx 1$ indicates an almost isotropic stencil while a large condition number indicates a highly stretched stencil. In all the computations here, the condition number is kept below 10.

10 Wall Boundary Scheme

On solid walls, the primitive variables are updated using the strong formulation [3]. For inviscid compressible flows, the strong formulation gives,

$$u_n = 0 \tag{33}$$

$$\frac{\partial H}{\partial n} = 0 \tag{34}$$

$$\frac{\partial S}{\partial n} = -\frac{\gamma - 1}{\rho^{\gamma - 1}} u_t \omega \tag{35}$$

$$\frac{\partial p}{\partial n} = -\rho \vec{n} \cdot (\vec{u} \cdot \nabla \vec{u}) \tag{36}$$

In the above equations, $S = p/\rho^{\gamma}$ is an entropy-like variable, H is the total enthalpy, ω is the vorticity, and n represents the direction normal to the wall. The value of any variable ϕ (S, H or p) on the wall can be obtained by enforcing the above conditions using,

$$\frac{\partial \phi}{\partial n} = n_x \frac{\partial \phi}{\partial x} + n_y \frac{\partial \phi}{\partial y} = Source \;\; term \tag{37}$$

where the x and y derivatives are replaced by their corresponding least squares expressions. Equation (35) is the Crocco relation in a direction normal to the wall, wherein the isenthalpy of the flow is assumed. The vorticity is everywhere zero if there are no discontinuities in the flow, and according to [3], enforcing zero normal entropy gradient on the wall is less dissipative for subsonic and transonic flows. Hence, this condition has been used in all the computations.

A relaxation procedure has been used in updating the variables on the wall. If $\bar{\phi}^{new}$ is the value obtained from (37), then we set,

$$\phi^{new} = \phi^{old} + \alpha(\bar{\phi}^{new} - \phi^{old})$$

where α is a relaxation factor, with typical value of $\alpha \leq 0.1$. The use of relaxation was found to be necessary for some cases with large gradients as in flow over a cylinder in order to preserve positivity of pressure and density.

11 Outer Boundary Scheme

In lifting potential flows, the asymptotic form of the solution is that due to a point vortex. In the case of flow past an airfoil at subsonic and transonic Mach numbers, the flow in the far-field can be assumed to be a uniform circulatory flow due to a point vortex placed at the center chord of the airfoil [10]. The circulation due to the vortex is related to the instantaneous lift through the Kutta-Jowkousky theorem,

$$\Gamma = \frac{1}{2} c |\vec{u}_\infty| C_L \tag{38}$$

The flow induced by the vortex is calculated from small perturbation theory with the effect of compressibility included through Prandtl-Glauert correction. This gives the velocity at the far-filed as,

$$u_f = u_\infty + k_f \sin\theta_f \tag{39}$$

$$v_f = v_\infty - k_f \cos\theta_f \tag{40}$$

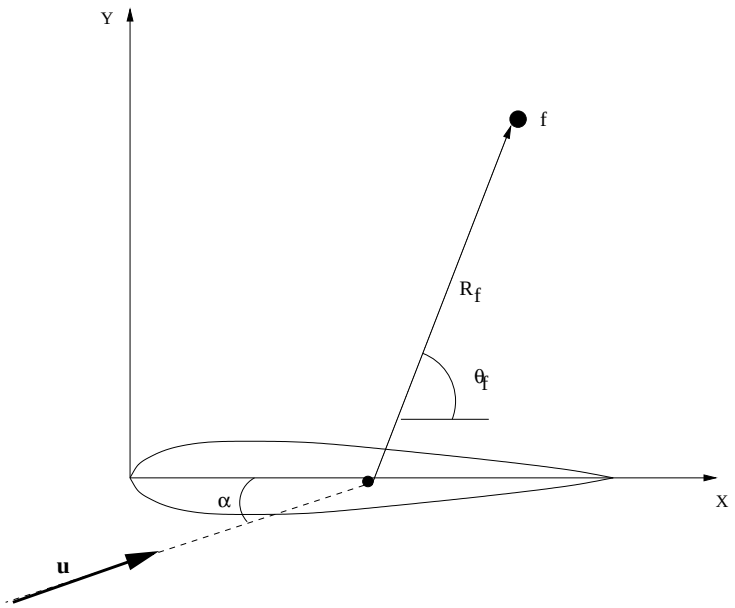

Figure 4: Point vortex model for far-field treatment

where k_f is given by,

$$k_f = \frac{\Gamma\sqrt{1-M_\infty^2}}{2\pi R_f(1-M_\infty^2\sin^2(\theta_f-\alpha))} \tag{41}$$

and

$$u_\infty = |\vec{u}_\infty|\cos\alpha, \quad v_\infty = |\vec{u}_\infty|\sin\alpha$$

The remaining unknowns are determined by enforcing the constancy of total enthalpy and assuming that the flow is isentropic in the far-field. This is a valid assumption in subsonic flows, and is quite reasonable in transonic flows provided the shocks do not reach the outer boundary. The point vortex model has been used for subsonic/transonic flow past NACA0012 and subsonic flow past a two-dimensional cylinder.

12 Results

The new method KRIME together with the boundary conditions described above has been applied to standard test cases. The first problem is a hypothetical 2-D blast wave problem, which is used to demonstrate the rotational invariance property. The initial conditions for this problem are,

$$(\rho,u,v,T) = \begin{cases} (1.2,0,0,5000) & \text{if } \max(|x|,|y|) \le 0.1 \\ (1.0,0,0,300) & \text{if } \max(|x|,|y|) \ge 0.1 \end{cases}$$

The computational domain is $[-1,1]\times[-1,1]$ and a Cartesian grid of size 101×101 was used. The solution is advanced through 600 time-steps with a constant time-step of $\Delta t = 10^{-6}$.

Configuration	NACA0012	Cylinder-1	Cylinder-2
Total points	9513	8052	12857
On body	200	200	200
On outer boundary	80	200	225

Table 1: Details of unstructured grids used in the computaions.

Interpolation is done using q-variables and weights are uniform. The computation is first done on the given grid, which we designate by the angle $\theta = 0$. Then the computation is repeated by first rotating all the quantities through some angle θ. We compare this result with the reference result of $\theta = 0$ by the following norms,

$$\begin{aligned} \|\phi(\theta)\|_1 &= \frac{1}{N}\sum_{i=1}^{N}\left|\frac{\phi_i(\theta)-\phi_i(0)}{\phi_i(0)}\right| \\ \|\phi(\theta)\|_2 &= \sqrt{\frac{1}{N}\sum_{i=1}^{N}\left(\frac{\phi_i(\theta)-\phi_i(0)}{\phi_i(0)}\right)^2} \\ \|\phi(\theta)\|_\infty &= \max_i\left|\frac{\phi_i(\theta)-\phi_i(0)}{\phi_i(0)}\right| \end{aligned}$$

If we set $\nabla q = 0$, then theorem (3) can be applied and the scheme is rotationally invariant. We have found that the norm of the solution difference in this case is zero upto machine precision. The pressure and density contours are given in figure (5) and (6) for $\theta = 0$ and $\theta = 30^0$ respectively. When $\nabla q \neq 0$, then theorem (3) is not valid since the min-max limiter is not rotationally invariant. However, we have computed the norm of the solution difference for different values of θ and these are shown in figure (7). The pressure and density contours are given in figure (8) and (9) for $\theta = 0$ and $\theta = 30^0$ respectively.

The other problems are standard 2-D aerodynamic flows over NACA0012 airfoil at different mach numbers and low subsonic and supersonic flow over a 2-D cylinder. An unstructured grid has been used in both the cases whose details are given in table (1). The min-max limiter of Barth-Jesperson has been used for the derivatives of the interpolation variables. The primitive variables have been used for the NACA0012 test cases and the entropy variables have been used for flow over cylinder.

The results of the computations are given in table (2) for flow over NACA0012. These agree pretty well with the AGARD and GAMM standards. The pressure contours, mach contours and the pressure distribution over the airfoil are shown in figures (10)-(15), which indicate that the scheme has captured all the essential features of the flows considered.

For flow over a cylinder, two different grids have been used for subsonic and supersonic flows. Cylinder-1 is used for subsonic flow and has a circular outer boundary while Cylinder-2 was used for supersonic flow and has a parabolic outer boundary, as shown in figure (19). Figures (16) shows the results for flow over a cylinder at a mach number of 0.3 which is a challenging test case for an Euler solver. Mathematically the flow should be symmetric

Mach No. and AOA	Computed		GAMM and AGARD	
	C_l	C_d	C_l	C_d
0.80, 1.25^o	0.3690	0.0213	0.363	0.023
0.85, 1^o	0.3839	0.0551	0.388	0.059
1.20, 0^o	-0.0009	0.0941	0.000	0.096

Table 2: Comparison of lift and drag coefficients for flow over NACA-0012.

about both the horizontal and vertical diameters of the cylinder. The contours show good symmetry about the horizontal diameter but not about the vertical diameter, which is due to the inherent numerical dissipation in the method leading to spurious entropy production. In figure (17), the pressure distribution over the cylinder has been compared with the results of potential theory. The total pressure and total temperature ratios at the stagnation point are 0.9973 and 1.0000 on the windward side. Figure (18) shows the pressure contours and mach number contours obtained for flow over a cylinder at $M_\infty = 3$. The bow shock on the front and the slip line on the rear of the cylinder have been captured. The entropy contours are shown in figure (19). The total pressure and total temperature ratios at the stagnation point behind the shock are 0.3232 and 1.0004 while the exact values are 0.3283 and 1 respectively.

13 Summary

A new rotationally invariant gridless method for Euler equations which does not require stencil splitting for enforcing upwinding has been described and tested on many standard problems. The results demonstrate the ability of the method in computing subsonic, transonic and supersonic flows. Much more work needs to be done in order to ascertain the merits and demerits of the new method in comparison with other gridless methods like LSKUM. We list down some relevant points that need to be addressed in a future study.

1. The method is formally only first order accurate but the results obtained are comparable to that of a second order method. The reason for this behaviour is not known at present.
2. The actual order of accuracy of the method is not known and must be determined through numerical experiments.
3. The use of min-max limiter spoils the rotational invariance of the method but this effect is small. If we use a smooth limiter unlike what is used here, we can expect to reduce this effect further. A rotationally invariant limiter might also be developed.
4. No information is available regarding the amount of numerical viscosity that is inherent in the method
5. The boundary conditions must be incorporated within the framework of the interior scheme.

6. The method must be tested on truly arbitrary distribution of points in order to demonstrate it's gridless nature.

References

[1] Balakrishnan. N and Praveen. C, *A New Upwind Least Squares Finite Difference Scheme (LSFD-U) for Euler Equations of Gas Dynamics*, Finite Volumes for Complex Applications-II, Hermes Science Publications, Paris, 1999, pp. 331.

[2] Balakrishnan. N, *New Least Squares Based Finite Difference Methods*, 99-FM-9, Dept. of Aerospace Engg., Indian Institute of Science, Bangalore.

[3] Balakrishnan, N. and Fernandez, G., *Wall Boundary Conditions for Inviscid Compressible Flows on Unstructured Meshes*, Int. J. Numer. Meth. Fluids, vol. 28, pp. 1481-1501, 1998.

[4] S. M. Deshpande, *On the Maxwellian Distribution, Symmetric Form, and Entropy Conservation for the Euler Equations*, NASA-TP-2583, 1986.

[5] Ghosh. A. K, *Robust Least Squares Upwind Method for Inviscid Compressible Flows*, PhD Thesis, Dept. of Aerospace Engg., Indian Institute of Science, Bangalore, June 1996.

[6] Koji Morinishi, *An Implicit Gridless Type Solver for the Navier-Stokes Equations*, Int. Symp. on CFD, Bremen, September 1999.

[7] Praveen. C, *A New Upwind Least Squares Finite Difference Scheme for Compressible Flows*, ME Thesis, Dept. of Aerospace Engg., Indian Institute of Science, Bangalore, January 2000.

[8] Praveen. C, *Some Results on the Least Squares Formula*, FM Report, FM 2001-06, Dept. of Aerospace Engg., IISc, Bangalore.

[9] V. Ramesh and S. M. Deshpande, *Euler Computations on Arbitrary Grids Using LSKUM*, First ICCFD, July 2000, Kyoto, Japan.

[10] Thomas, J. L. and Salas, M. D., *Far-Field Boundary Condition for Transonic Lifting Solutions to the Euler Equations*, AIAA Paper No. 85-0020, 1985

A The choice $f_I = (f_o + f_i)/2$

It is easy to show that this particular choice gives a consistent formula since it is 1-exact.

$$f_i = f_o + (2\Delta x_I) f_{xo}^{ex} + \frac{(2\Delta x_I)^2}{2} f_{xxo}^{ex} + O({\Delta x_I}^3)$$

$$f_I = f_o + (\Delta x_I) f_{xo}^{ex} + (\Delta x_I)^2 f_{xxo}^{ex} + O({\Delta x_I}^3)$$

Also,

$$f_I^e = f_o + (\Delta x_I) f_{xo}^{ex} + \frac{(\Delta x_I)^2}{2} f_{xxo}^{ex} + O(\Delta {x_I}^3)$$

so that,

$$f_I - f_I^e = -\frac{(\Delta x_I)^2}{2} f_{xxo}^{ex} + O(\Delta {x_I}^3) = O(\Delta {x_I}^2)$$

which shows that this particular choice is 1-exact or 2^{nd}-order accurate. But this does not give an upwind approximation. The choice,

$$f_I = \begin{cases} f_L, \text{ if } v \geq 0 \\ f_R, \text{ if } v \leq 0 \end{cases}$$

is upwind but leads to an inconsistent formula since this is only 0-exact.

B Expressions for Split Fluxes

The expressions for the split fluxes as defined in equation (22) are given below.

$$\tilde{G}^{\pm} = \begin{bmatrix} \rho u_2 A_1^{\pm} \\ \rho u_2 (u_1 A_1^{\pm} \pm B_1) \\ (p + \rho u_2^2) A_1^{\pm} \\ (E+p) u_2 A_1^{\pm} \pm \dfrac{\rho u_1 u_2}{2} B_1 \end{bmatrix}$$

The fluxes $F^{\pm}$ are the usual kinetic x-split fluxes, which are given by,

$$F^{\pm} = \begin{bmatrix} \rho (u_1 A_1^{\pm} \pm B_1) \\ (p + \rho u_1^2) A_1^{\pm} \pm \rho u_1 B_1 \\ \rho u_2 (u_1 A_1^{\pm} \pm B_1) \\ (E+p) u_1 A_1^{\pm} \pm (E + p/2) B_1 \end{bmatrix}$$

where

$$E = \frac{p}{\gamma - 1} + \frac{\rho |\vec{u}|^2}{2}$$

and for $\alpha = 1, 2$,

$$\begin{aligned} s_\alpha &= u_\alpha \sqrt{\beta} \\ A_\alpha^{\pm} &= \frac{1}{2} [1 \pm \operatorname{erf}(s_\alpha)] \\ B_\alpha &= \frac{\exp(-s_\alpha^2)}{2\sqrt{\pi \beta}} \end{aligned}$$

Pressure

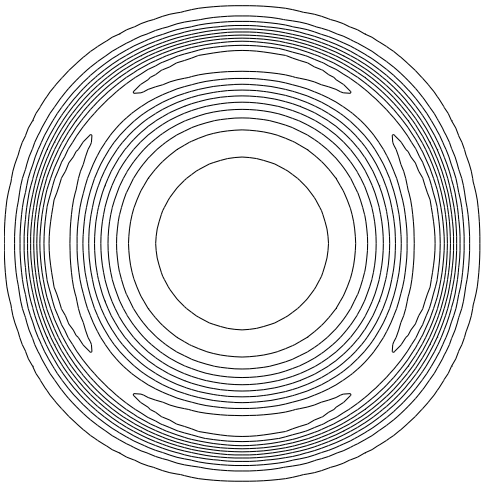

Figure 5: Contours for blast wave problem using inconsistent scheme at reference angle 0^o.

Pressure

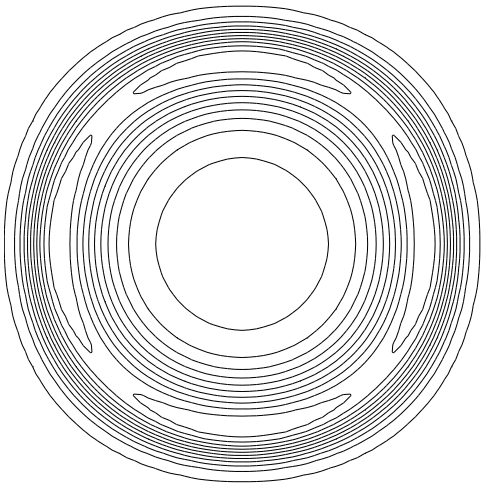

Figure 6: Contours for blast wave problem using inconsistent scheme at reference angle 30^o.

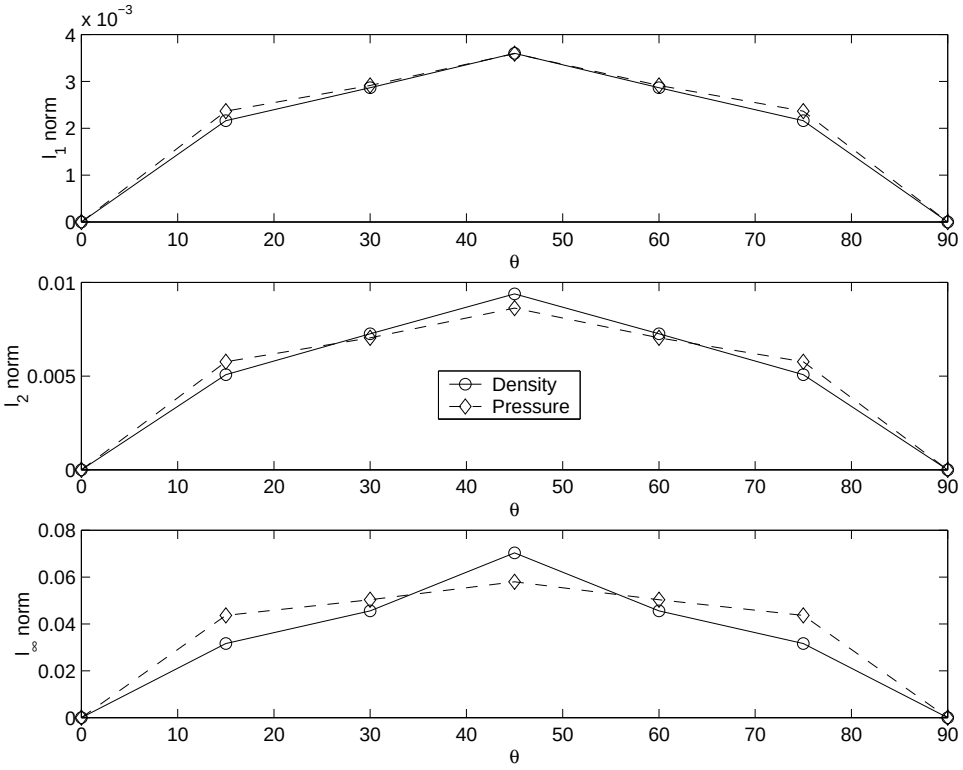

Figure 7: Norm of the solution difference for blast wave problem.

Pressure

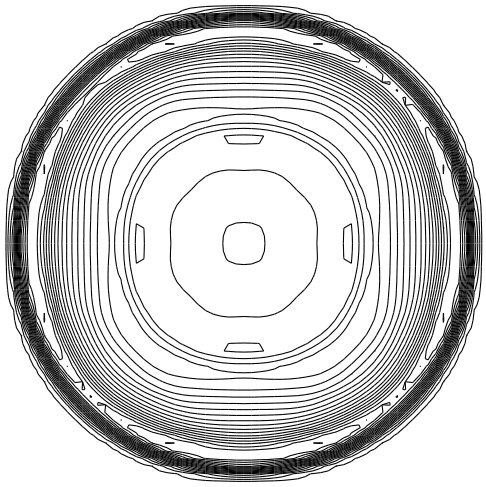

Figure 8: Contours for blast wave problem using first order scheme at reference angle 0^o.

Pressure

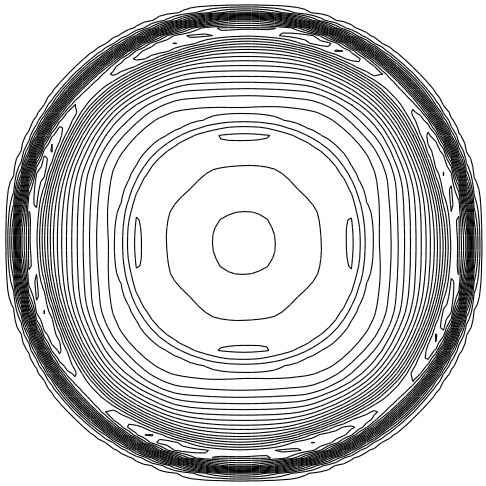

Figure 9: Contours for blast wave problem using first order scheme at reference angle 30^o.

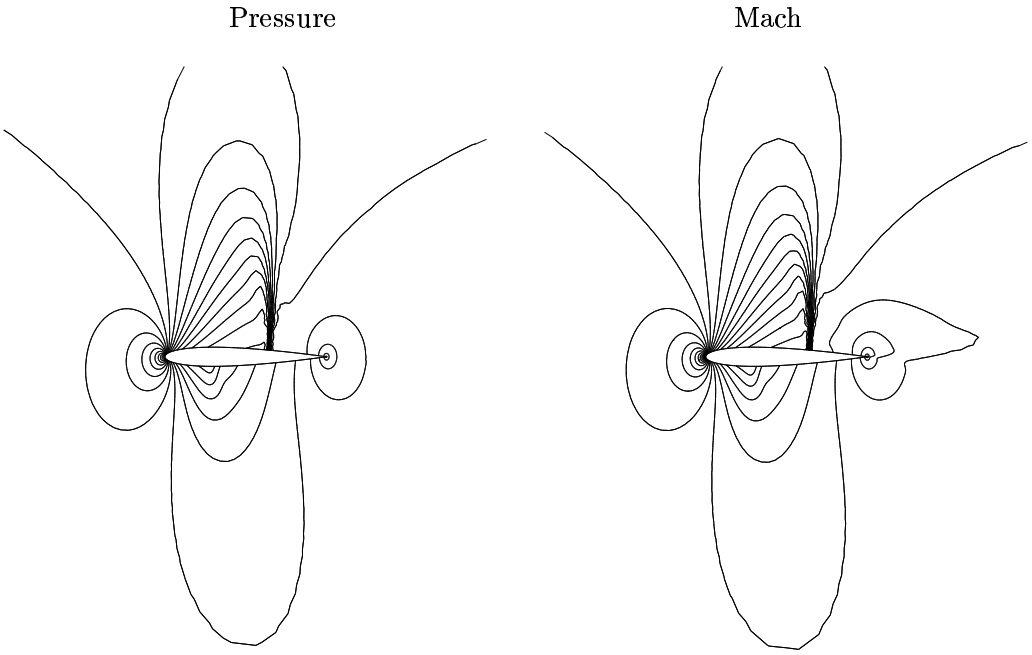

Figure 10: Pressure and Mach contours $M_\infty = 0.80$, $\alpha = 1.25^o$.

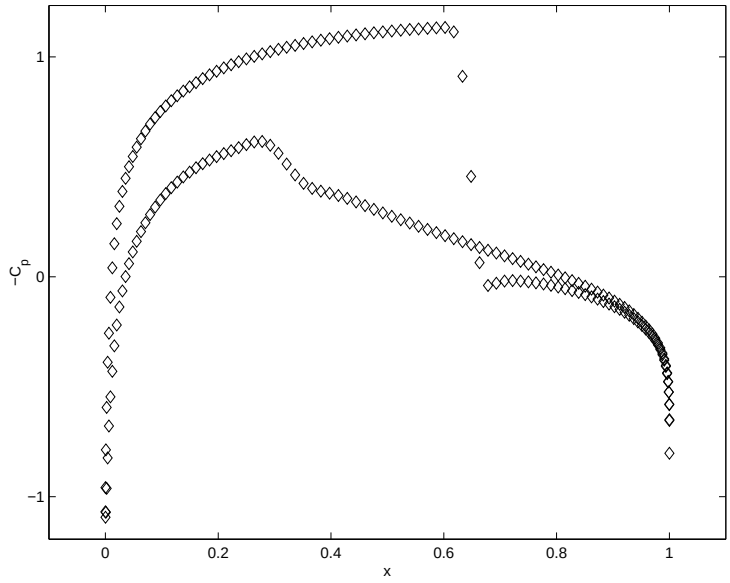

Figure 11: Pressure distribution on airfoil $M_\infty = 0.80$, $\alpha = 1.25^o$.

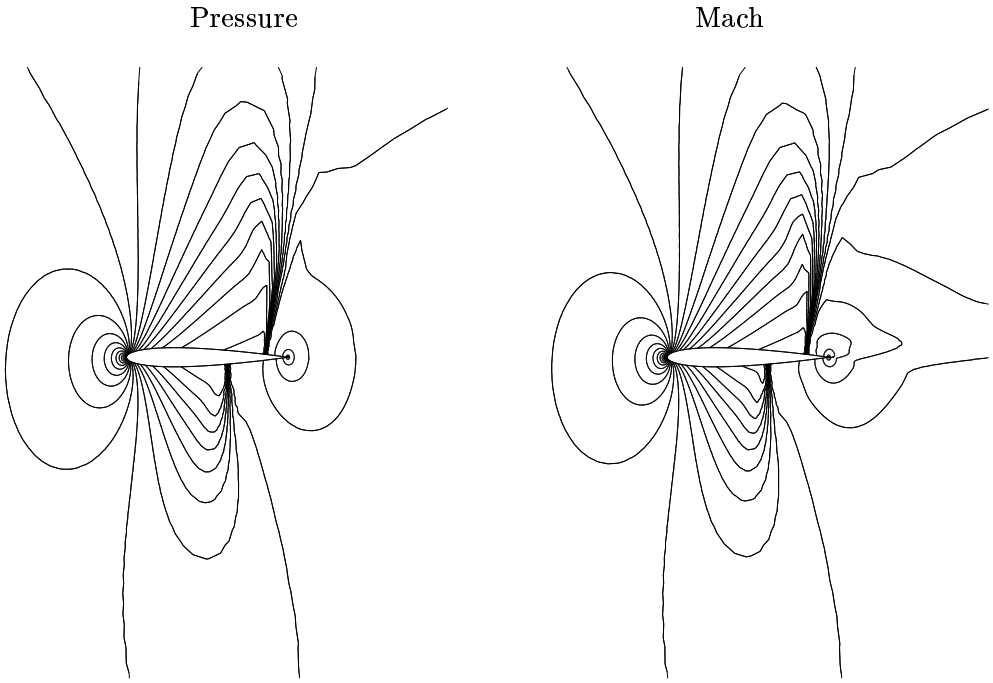

Figure 12: Pressure and Mach contours for $M_\infty = 0.85$, $\alpha = 1.0^o$.

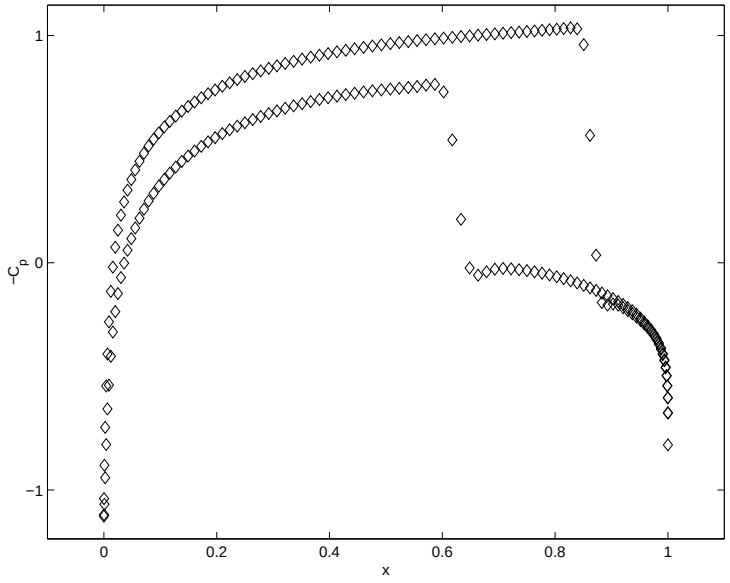

Figure 13: Pressure distribution on airfoil $M_\infty = 0.85$, $\alpha = 1.0^o$.

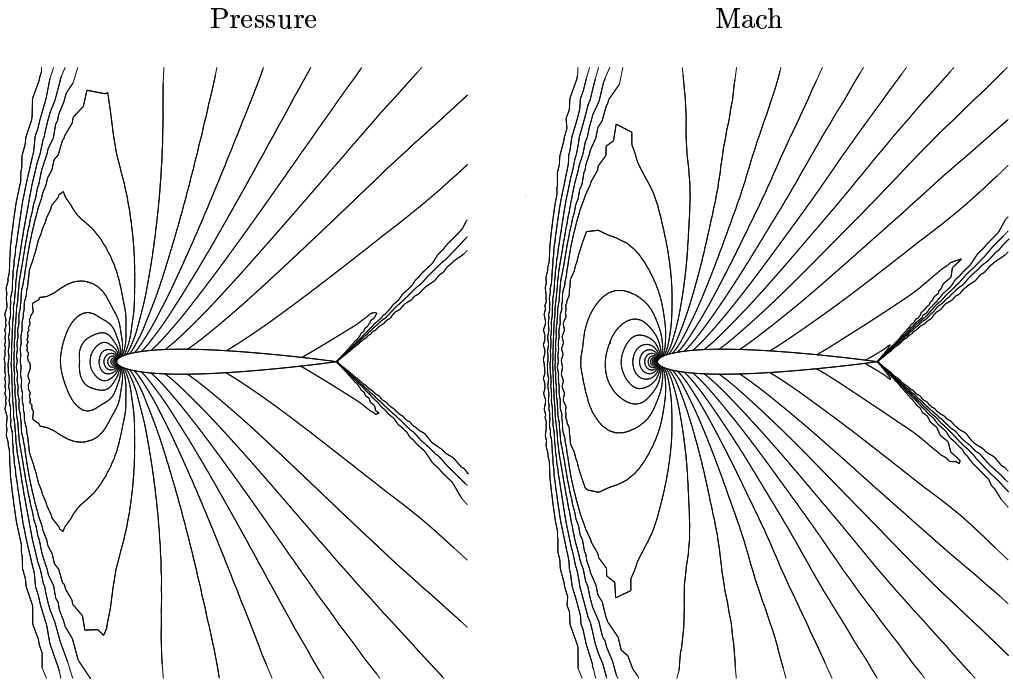

Figure 14: Pressure and Mach contours for $M_\infty = 1.20$, $\alpha = 0.0^o$.

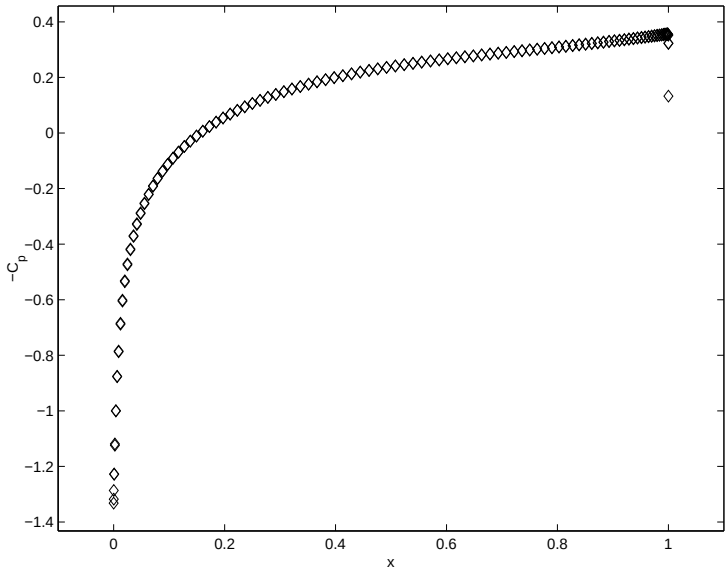

Figure 15: Pressure distribution on airfoil $M_\infty = 1.20$, $\alpha = 0.0^o$.

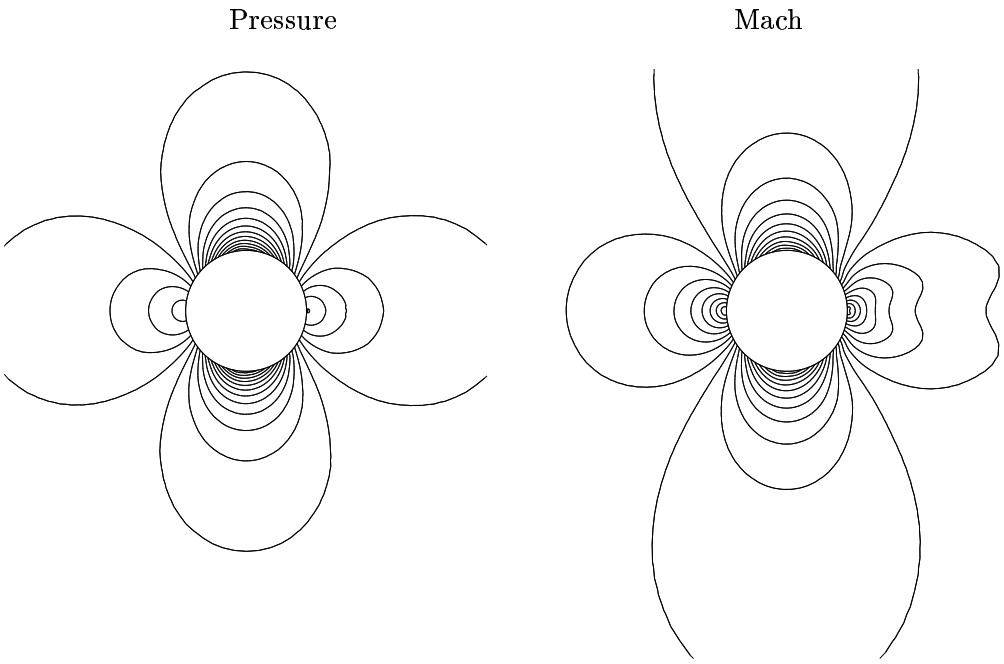

Figure 16: Pressure and Mach contours for $M_\infty = 0.3$, $\alpha = 0.0^o$.

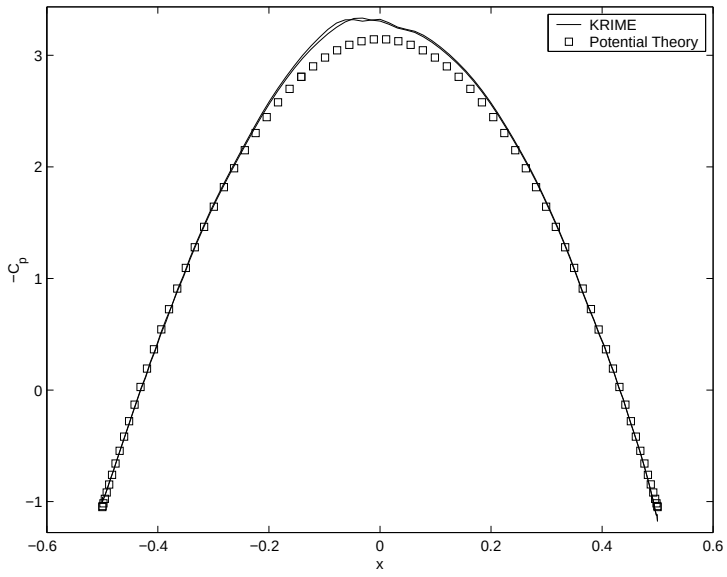

Figure 17: Pressure distribution on cylinder; $M_\infty = 0.3$, $\alpha = 0.0^o$.

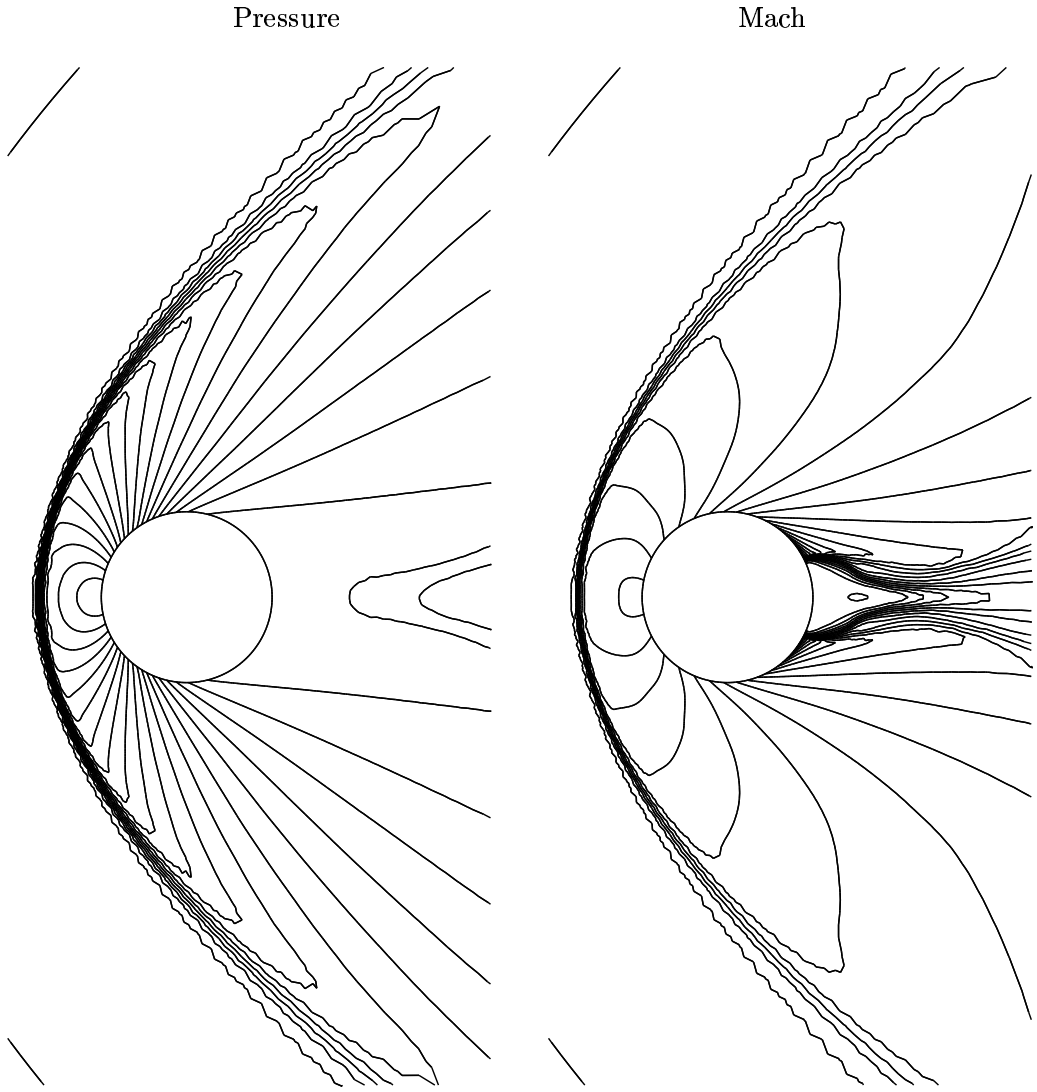

Figure 18: Pressure and Mach contours for flow over a cylinder; $M_\infty = 3$, $\alpha = 0.0^o$.

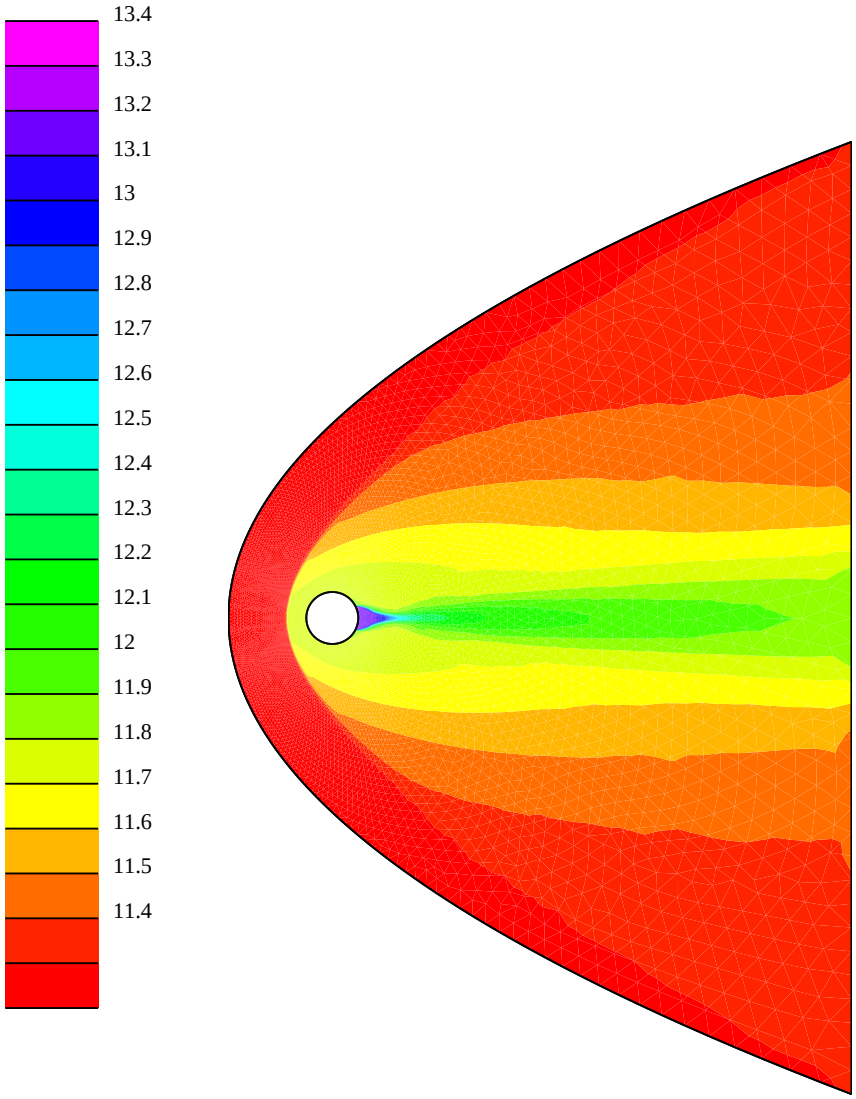

Figure 19: Entropy contours, $M_\infty = 3$, $\alpha = 0.0^o$.